

Non-diffracting light in nature: Anomalously reflected self-healing Bessel beams from jewel scarabs

Cite as: APL Photonics 4, 126102 (2019); <https://doi.org/10.1063/1.5125045>

Submitted: 20 August 2019 . Accepted: 10 November 2019 . Published Online: 02 December 2019

Petr Bouchal , Josef Kapitán , Martin Konečný , Marek Zbončák, and Zdeněk Bouchal 



View Online



Export Citation



CrossMark

ARTICLES YOU MAY BE INTERESTED IN

Floquet topological insulator laser


APL Photonics 4, 126101 (2019); <https://doi.org/10.1063/1.5121414>

Determining the complex Jones matrix elements of a chiral 3D optical metamaterial

APL Photonics 4, 126107 (2019); <https://doi.org/10.1063/1.5127169>

Advances in hydrogel photonics and their applications

APL Photonics 4, 120901 (2019); <https://doi.org/10.1063/1.5122780>



AMERICAN ELEMENTS
THE ADVANCED MATERIALS MANUFACTURER®

additive manufacturing epitaxial crystal growth cerium oxide polishing powder silver nanoparticles sputtering targets III-IV semiconductors CVD precursors europium phosphors
 gallium lump glassy carbon nanodispersions InAs wafers laser crystals ultra high purity materials MOFs
 surface functionalized nanoparticles organometallics quantum dot rare earth metals photovoltaics refractory metals MOCVD
 superconductors transparent ceramics ultra high purity silicon

American Elements opens up a world of possibilities so you can **Now Invent!**

Over 15,000 certified high purity laboratory chemicals, metals, & advanced materials and a state-of-the-art Research Center. Printable GHS-compliant Safety Data Sheets. Thousands of new products. And much more. All on a secure multi-language "Mobile Responsive" platform.

deposition slugs OLED Lighting spintronics solar energy
 osmium nanoribbons thin films chalcogenides AuNPs
 GDC Li-ion battery electrolytes 99.999% ruthenium spheres
 endohedral fullerenes copper nanoparticles diamond micropowder
 CIGS MBE grade materials palladium catalysts flexible electronics
 beta-barium borate borosilicate glass dysprosium pellets YBCO
 pyrolytic graphite 3d graphene foam indium tin oxide mesoporous silica
 raman substrates sapphire windows tungsten carbide InGaAs
 barium fluoride carbon nanotubes lithium niobate scandium powder

Now Invent.™
The Next Generation of Material Science Catalogs

perovskite crystals yttrium iron garnet alternative energy h-BN
 gold nanocubes graphene oxide macromolecules photonics
 rhodium sponge fiber optics beamsplitters infrared dyes zeolites
 fused quartz metallocenes platinum ink buckyballs Ti-6Al-4V

www.americanelements.com



Non-diffracting light in nature: Anomalously reflected self-healing Bessel beams from jewel scarabs

Cite as: APL Photon. 4, 126102 (2019); doi: 10.1063/1.5125045

Submitted: 20 August 2019 • Accepted: 10 November 2019 •

Published Online: 2 December 2019



View Online



Export Citation



CrossMark

Petr Bouchal,^{1,2,a)}  Josef Kapitán,³  Martin Konečný,^{1,2}  Marek Zbončák,² and Zdeněk Bouchal³ 

AFFILIATIONS

¹Institute of Physical Engineering, Faculty of Mechanical Engineering, Brno University of Technology, Technická 2, 616 69 Brno, Czech Republic

²Central European Institute of Technology, Brno University of Technology, Purkyňova 656/123, 612 00 Brno, Czech Republic

³Department of Optics, Palacký University, 17 listopadu 1192/12, 771 46 Olomouc, Czech Republic

^{a)}Author to whom correspondence should be addressed: petr.bouchal@vutbr.ceitec.cz

ABSTRACT

We report a study of spatial light modulation in the photonic structure of jewel scarabs, revealing the interplay of the polarization and phase control of light, which is not possible with the current optical technology. Phase measurements performed on jewel scarabs demonstrate that the polarization anomalous (helicity-preserving) reflection of light occurs together with alteration of the dynamic phase associated with the optical path length. This control of light differs from the operation of artificially prepared polarization-sensitive structures, shaping light through the geometric phase altered by the polarization transformation. Challenging three-dimensional imaging of the cuticle, requiring high-resolution quantitative mapping of steep phase changes, has been achieved owing to the optical performance of recently developed geometric-phase microscopy. We find that the cuticle of jewel scarabs is formed of micrometer-sized axicon cells, generating thousands of Bessel beams with subwavelength spot size. The nondiffracting features and the self-healing ability of the Bessel beams originating from the beetle *Chrysina gloriosa* are demonstrated experimentally. Considering Bragg reflection and shaping of RGB components of white light Bessel beams, we explain the spatial structuring of colors in microscopic images of jewel scarabs and reveal the conversion of colors when changing the distance from the cuticle. The functionality and performance of the cuticle axicon cells are discussed in comparison with high-aperture dielectric meta-axicons, and potential applications in colorimetric refractive index sensing are outlined.

© 2019 Author(s). All article content, except where otherwise noted, is licensed under a Creative Commons Attribution (CC BY) license (<http://creativecommons.org/licenses/by/4.0/>). <https://doi.org/10.1063/1.5125045>

I. INTRODUCTION

An exceptional diversity of natural phenomena, including high reflectivity or transmissivity, polarization selectivity, dichroism, iridescence, or structural color, is achieved through the interaction of light with photonic structures of great morphological variability.^{1,2} In the insect kingdom, iridescent beetles that preferentially reflect light with left-handed circular polarization (LHCP) have garnered much interest.^{3,4} The cuticles of these beetles comprise clusters of chitin microfibrils capable of self-organization into a helicoidal Bouligand structure,^{5,6} with properties similar to the cholesteric

liquid crystal phase.^{7,8} In this structure, the microfibrils are aligned parallel in a plane, and the orientation between adjacent planes is slightly twisted. Light with LHCP is selectively reflected within the spectral bandwidth given by the birefringence and the pitch of the structure,⁹ and broadband reflection may take place when the pitch varies across the cuticle.^{10–13} The anomalous reflection of light has also been widely examined in relation to animal behavior^{14,15} and as part of an extensive study of photonics in nature.^{16,17} Structural coloration, arising as a result of Bragg reflection from helicoidally stacked cellulose microfibrils that form layers in the cell walls of the epicarp, has also been examined in plants.¹⁸

In addition to the well-understood polarization selectivity, light reflected from jewel scarabs is influenced by modulation of the dynamic phase. Although the spatially varying phase alteration has a significant impact on the structural coloration, this effect has not yet been fully explored. Information on phase response has been deduced from imaging of the cross sections of the outer and inner exocuticles.^{19,20} This technique provides the geometric shape of the cuticle only in a single plane, and the cutting causes anisotropic propagation of fractures and artifacts from the microtome knife.^{21,22} Progress in the imaging of cuticle cells has been achieved through the application of laser scanning confocal microscopy. Using beetle autofluorescence, concentric nested arcs on the surface of a cone were discovered within individual hexagonal cells, and their structural analogy with cholesteric focal conic domains formed spontaneously on the free surface was inferred.⁸ In subsequent research, this hypothesis was revised when it was found that the cuticle of jewel scarabs comprises concave cells.¹¹

In our study, we apply the principles of holographic microscopy to demonstrate nondestructive quantitative phase imaging of the outer layer of the exocuticle. Holographic images enable reconstruction of the complex amplitude of light reflected from the cuticle, which was previously achievable only via numerical simulations.²³ The implemented high-resolution phase imaging provides wide-field (nonscanning) mapping of the cuticle, allowing the reconstruction of the three-dimensional (3D) shape of individual cells. The results of our measurements reveal the conical shape of the cuticle cells and show that these cells change the optical path of light as micrometer-sized reflective axicons. By modulating the dynamic phase of light, the axicon cells generate thousands of nondiffracting (ND) beams. These naturally created beams are proven to be Bessel beams, which have previously only been generated in laboratories,²⁴ and their self-healing ability is experimentally demonstrated. Using the present findings, a computational model is created using Bragg reflection and Bessel beam formation to explain structured coloration in microscopic images of the cuticle of jewel scarabs.

II. METHOD

The measurements were performed on a *Chrysina gloriosa* beetle, as shown in Figs. 1(a) and 1(b). Experiments were conducted using geometric-phase microscopy, a technique that has recently been used successfully for quantitative phase imaging of plasmonic metasurfaces,²⁵ as well as live cell imaging and phase monitoring of liquid crystals.²⁶ The measurement was carried out in the area of the cuticle that appears bright green in LHCP light [Fig. 1(a)]. The magnified bright-field image of this area (Melles Griot 50 \times , NA = 0.55, 2 \times focal extender) shows hexagonal cells whose 3D shape is measured here. In the phase measurement performed by geometric-phase microscopy, Köhler illumination of the sample is used (tungsten-halogen lamp, bandpass filter with central wavelength $\lambda = 500$ nm, full width at half maximum 50 nm). The illumination path is supplemented by a circular polarizer so that the light incident on the beetle has LHCP. The illuminating light with LHCP is partially reflected by the wax layer that covers the cells of the cuticle and partially transmitted through the air-wax interface. The polarization of the light reflected by the wax layer is changed from LHCP to right-handed circular polarization (RHCP), while its phase

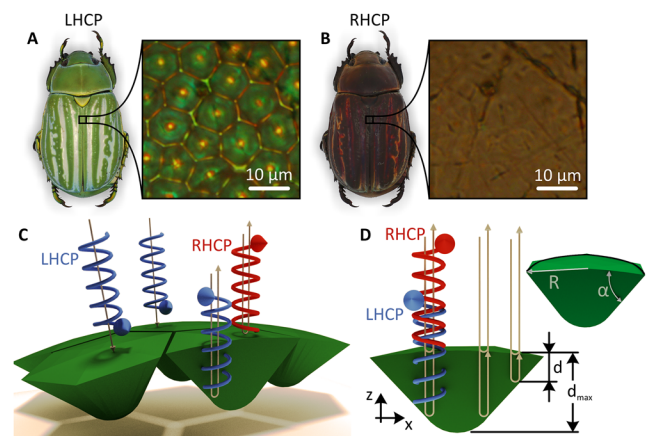


FIG. 1. Principles of quantitative phase imaging of the outer layer of the exocuticle of the *Chrysina gloriosa* beetle by geometric-phase microscopy. Photographs and bright-field microscopy images taken under illumination by light with (a) LHCP and (b) RHCP. (c) Normally reflected reference field with RHCP (red color) and anomalously reflected signal field with LHCP (blue color) when the cells of the exocuticle are illuminated with LHCP light. (d) Difference in the geometric path d introduced between the reference and signal fields.

remains smooth [the RHCP bright field image is shown in Fig. 1(b)]. The RHCP light reflected by the wax layer is used as a reference wave in the phase measurement. The light penetrating through the wax layer is anomalously reflected⁴ from the bottom of the cells. This light maintains LHCP and yields information about the shape of individual cells [Figs. 1(c) and 1(d)]. Hence, although the reflected light comprises both LHCP and RHCP waves, illumination with only LHCP was used. All the reflected light is captured by the microscope objective (Nikon 100 \times , NA = 0.9) and directed toward the tube lens (Nikon CFI60) and the add-on imaging module, providing a polarization-selective transformation of the geometric (Pancharatnam-Berry) phase of light^{25,26} (supplementary material, Materials and Methods). The light reflected at the point of the wax layer (reference field) is correlated with the slightly defocused light reflected from the underlying chitin layers of the cell (signal field). The phase difference $\Delta\Phi$ introduced between the reference and signal fields is reconstructed from the temporal coherence function provided by the off-axis point hologram recorded by a CCD.^{25,26} As the refractive index of the wax is known, the local depth d of the measured cell may be determined from $\Delta\Phi$ [Fig. 1(d)]. The off-axis point holograms are simultaneously recorded for all points of the field of view; therefore, the 3D shape of all cells is reconstructed in a single shot.

III. RESULTS

A. Quantitative phase imaging of cuticle cells

The phase map illustrating the spatial variation of $\Delta\Phi$ introduced in the green area of the cuticle (field of view $30 \times 30 \mu\text{m}^2$) is shown in Fig. 2(a). By applying phase unwrapping, the 3D shape of individual cells was determined [Fig. 2(b)]. The projections in x - z and y - z planes [Figs. 2(c) and 2(d)] document the axicon shape of the individual cells. To verify the results, one of the cells was cut (Ultramicrotome Leica EM UC7) and the cross section obtained by

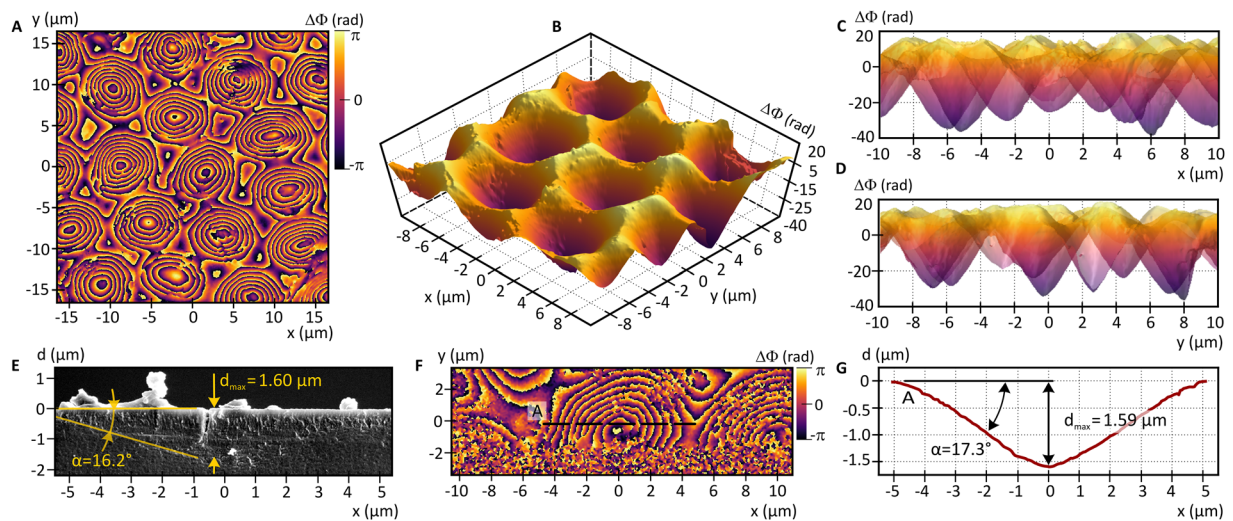


FIG. 2. Results of the phase measurement by geometric-phase microscopy and comparison with results obtained by scanning electron microscopy (SEM). (a) Spatial variation of the phase in the exocuticle cells. (b) Three-dimensional phase shape of the cells. [(c) and (d)] Projections of the measured phase in the x-z and y-z planes. (e) Cross section of a single axicon cell with depth d_{\max} and base angle α determined by SEM measurement. (f) Phase map of the cell used in SEM imaging (bottom half cut off). (g) Cross section of the cell along line A with d_{\max} and α obtained from the phase measurement.

scanning electron microscopy (FIB-SEM, Tescan Lyra3) [Fig. 2(e)] was compared with the phase measurement [Fig. 2(g)] (supplementary material). The depth and the base angle of the axicon profile determined by both methods were found to agree, although slightly different profiles were evaluated [the cross section in Fig. 2(g) was restored along line A of the phase map in Fig. 2(f)].

B. Demonstration of self-healing Bessel beams from *Chrysin gloriosa*

The finding that the cells represent reflective micrometer-sized axicons suggests the occurrence of ND beams in the light reflected from the cuticle. The structure of the reflected light is significantly influenced by the cuticle illumination, but the optical functionality of individual cells is well documented using monochromatic plane wave illumination. Through this approach, the response of a single axicon cell could be explored in detail because its complex transmission function was determined by the phase measurement. The phase and amplitude of one of the cells are shown in Figs. 3(a) and 3(b). Modifying the monochromatic plane wave ($\lambda = 500$ nm) by the measured phase and amplitude, the diffracted field was obtained by numerically solving the Kirchhoff diffraction integral. The 3D intensity distribution and the spots at three different distances are shown in Figs. 3(c) and 3(d). Although the cell surface is cracked [Fig. 3(f)], the disturbed beam intensity is gradually restored (the self-healing effect, examined later), as shown in Fig. 3(e). The light reflected by the cell represents a light needle beam with a mean spot radius of $r_0 = 0.25$ μm . The central spot is surrounded by several rings, and its shape and size remain unchanged during propagation to a distance of $L = 1.2$ μm (this axial range exceeds four times the depth of field of a diffraction limited lens with $\text{NA} = 1.34$, which creates an Airy disk with a 0.25 μm radius). To assess the parameters of the restored beam using the concept of ND beams, the basic parameters of the cell

are required, including the refractive index of the wax filling the cell ($n = 1.41$),^{27,28} the radius of the circle inscribed in the hexagonal cell R , and the axicon base angle α . This angle is given by R and the geometric depth of the cell provided by the phase measurement, $\alpha = \arctan(d_{\max}/R)$ [Fig. 1(d)]. Using the selected cell with $R = 3$ μm and measured phase depth $\Delta\Phi_{\max} = 38$ rad [Fig. 3(a)], the geometric depth was calculated from $d_{\max} = \lambda\Delta\Phi_{\max}/4\pi n$

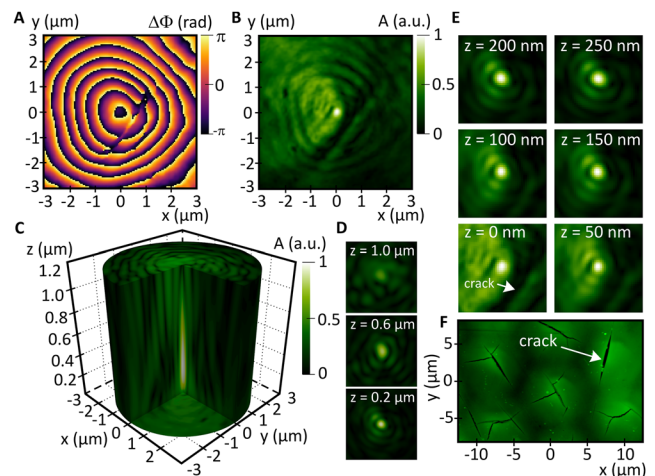


FIG. 3. Restoration of the Bessel beam from data measured in a single axicon cell. Measured (a) phase and (b) amplitude of the axicon cell of the exocuticle of *Chrysin gloriosa* used in the Kirchhoff numerical reconstruction of the (c) three-dimensional intensity of the Bessel beam and (d) intensity spots at different propagation distances. (e) Gradual restoration of the Bessel beam disturbed by a crack (f) in the cuticle cell [measured by atomic force microscopy (AFM) using an Icon Dimension (Bruker)].

($d_{max} = 1.07 \mu\text{m}$). The connection between the parameters of the reconstructed beam and the axicon cell was found using the Bessel beam model (supplementary material, Materials and Methods). The complex amplitude of the Bessel beam propagating along the z -axis is given by $E(r, z) \propto J_0(kr \sin \theta) \exp(ikz \cos \theta)$, where $k = 2\pi/\lambda$, r is the radial cylindrical coordinate, J_0 denotes the zero-order Bessel function of the first kind, and the angular parameter is given by $\theta = \arcsin(n \sin 2\alpha)$ (the parameter $NA_a = \sin \theta$ is referred to as the axicon numerical aperture²⁹). The beam spot radius can be determined from the first zero point of the Bessel function, $r_0 = 0.381\lambda/\sin \theta$. The ideal Bessel beam carries an infinite energy, and its spot intensity remains unchanged over an unlimited range of propagation. The beam created by an axicon cell suppresses the spreading due to diffraction within a bounded interference region, as shown in Fig. 4(c). The length L of this area depends on the cell radius, $L = R/\tan \theta$.²⁴ With $n = 1.41$ and $\alpha = 19.63^\circ$, giving $\theta = 63.16^\circ$ ($NA_a = 0.9$), the resulting beam parameters are $r_0 = 0.21 \mu\text{m}$ and $L = 1.52 \mu\text{m}$. These values correspond well to the parameters of the beam reconstructed from the amplitude and phase measured in the axicon cell ($r_0 = 0.25 \mu\text{m}$, $L = 1.2 \mu\text{m}$), demonstrating the applicability of the Bessel beam approach.

The unique properties of ND beams result from the specific form of their spatial spectrum, which is composed of plane waves whose wave vectors form a conical surface (supplementary material, Materials and Methods). Because the plane waves forming the Bessel beam are inclined relative to the beam axis, the energy of these waves can pass around a nontransparent obstacle inserted

into the beam path, allowing self-healing of the disturbed beam³⁰ [Fig. 4(c)]. This capability has been widely examined and used in optical manipulation³¹ and microscopy.³²

To demonstrate self-healing using the Bessel beam generated by an axicon cell of a *Chrysina gloriosa* beetle, submicrometer-sized steel grains were used as nontransparent obstructions disturbing the beam spot. The Bessel beam created just behind the axicon cell overlaps with the illumination beam; hence, the self-healing was demonstrated in the image space of the original beam. The array of Bessel beams, imaged using a standard microscope with water immersion and cover glass (Nikon 100 \times , NA = 0.9), is shown in Fig. 4(a) together with the spatial spectrum obtained in k -space by an optical Fourier transform. The axial intensity cross section of a single beam in Fig. 4(b) was obtained by moving the cuticle with a piezoelectric transducer and sequentially capturing the beam spots on a CCD. Immersion and cover glass were used to enlarge the axial range of the beam up to $35 \mu\text{m}$ (detailed in the supplementary material). A slight expansion of the beam profile during the propagation occurs because the illumination of the cell violates the condition of single plane-wave incidence (supplementary material). In the self-healing experiments, steel grains were placed in the back focal plane of the tube lens, where the image of the Bessel beam array was created [the spot of one of the beams is shown in the left panel of Fig. 4(d)]. Using a fine transverse adjustment, the central spot of the selected Bessel beam was almost completely blocked by the steel grain, as shown in Fig. 4(d). At a distance of 270 nm , the bright center was again evident, while the original Bessel spot was fully restored

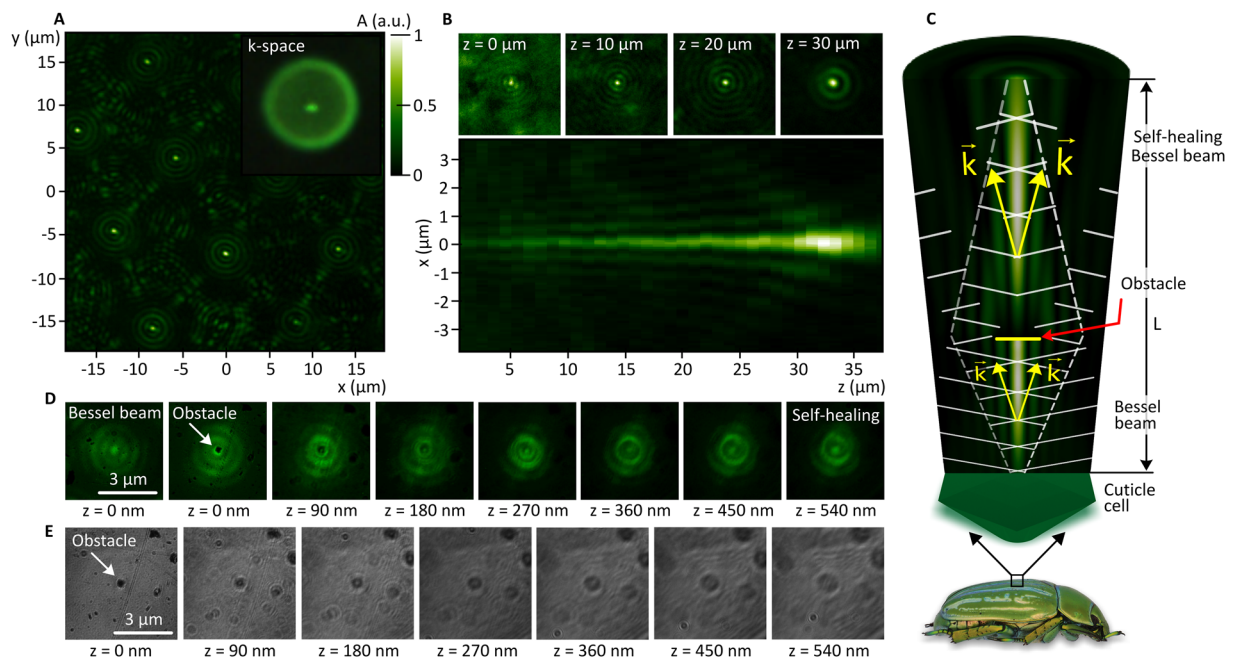


FIG. 4. Optical imaging and self-healing of Bessel beams generated by axicon cells of the *Chrysina gloriosa* beetle (Nikon 100 \times , NA = 0.9, water immersion and cover glass). (a) Array of Bessel beams created by individual cells and the spatial spectrum measured in k -space (optical Fourier transform of the beam array). (b) Cross section of the propagating Bessel beam and its spots at different distances. (c) Principle of the self-healing of a Bessel beam. (d) Generated Bessel beam (left panel) and snapshots illustrating the spot disturbed by an obstacle (steel grain) and its gradual restoration to its original form. (e) Propagation of a collimated light beam behind a nontransparent obstacle (steel grain).

at 540 nm. For comparison, the propagation of a collimated light beam distorted by the same obstacle is shown in Fig. 4(e). A natural manifestation of the self-healing effect occurs in beams emanating from cuticle cells damaged by cracks [Fig. 3(f)]. Beams that display significant disturbances in intensity near the surface of the cell gradually acquire a symmetrical Bessel-like spot during free propagation, as demonstrated in Fig. 3(e).

C. Modeling and measuring spatially structured coloration

Under white light illumination, a rich variety of color effects, including iridescence and structural coloration, are manifested in the light reflected by jewel scarabs. Although iridescence has been widely investigated, understanding of the structural coloration has been limited by the lack of information on the 3D shape of cuticle cells. Our phase measurement reveals that the cells are reflective micrometer-sized axicons that generate nondiffracting Bessel beams and create colored spots in microscopy images of the cuticle. In previous studies of structural coloration, the shape of the cells was deduced from cross-sectional slices that predicted a concave shape of the cells¹¹ (conic sections give a parabolic or hyperbolic profile). The model presented here simulates white light images produced by photonic structures in which Bragg reflection, multi-layer interference, and generation of Bessel beams are collectively manifested. This model was applied to investigate the *Chrysina gloriosa* beetle, specifically its cuticle areal structure that forms green stripes composed of hexagonal cells [photograph and microscopy image in Fig. 1(a)].

The incident LHCP light penetrates through the wax layer and, because of Bragg reflection from the underlying layers, returns whilst maintaining LHCP. The upper layer is not planar, but consists of the axicon cells that are also replicated in the lower layers (supplementary material, Fig. S2). In the area of a single cuticle cell bounded by the aperture function A , the light reflected from the individual layers is superposed coherently if the optical path difference does not exceed the coherence length. The light reflected from the m th layer is obtained from the incident light by modifying its amplitude and phase by $t_m = a_m(\lambda)A(\vec{r}_\perp)\exp[i\Phi(\vec{r}_\perp, \lambda) + i\delta_m(\lambda)]$, where $\vec{r}_\perp = (x, y)$, a_m and δ_m are the reflection coefficient and the phase shift of the m th layer, respectively, and Φ denotes a spatially varying phase imposed on the light by the axicon cell. In the simulations shown here, perpendicular illumination of the cuticle was considered and δ_m was determined by the optical thickness of the layers. When investigating iridescence, the change in a_m and δ_m with the angle of the incident light must be considered. For an ideal reflective axicon, Φ has rotational symmetry and varies linearly with $r = \sqrt{x^2 + y^2}$. When examining the real cuticle cells, the value of $\Phi = \Delta\Phi$ determined by measurement is used in simulations.

At the surface of the cuticle, the resulting reflected light can be represented by the following:

$$E_0(\vec{r}_\perp, \lambda) = w(\lambda)A(\vec{r}_\perp)\exp[i\Phi(\vec{r}_\perp, \lambda)],$$

where w denotes the interference of the light reflected by M layers,

$$w(\lambda) = \sum_{m=1}^M a_m(\lambda)\exp[i\delta_m(\lambda)].$$

The light field at a distance z from the cuticle is given by the Kirchhoff diffraction integral with the kernel K :

$$E(\vec{r}_\perp, z, \lambda) = w(\lambda) \iint A(\vec{r}'_\perp)\exp[i\Phi(\vec{r}'_\perp, \lambda)]K(\vec{r}'_\perp, \vec{r}_\perp, z, \lambda)d\vec{r}'_\perp.$$

The resulting color image created by the cuticle cell under white light illumination arises as an incoherent superposition of the images obtained with red (R), green (G), and blue (B) colored light. The intensity I_{RGB} of this image can be written as

$$I_{RGB}(\vec{r}_\perp, z) = I(\vec{r}_\perp, z, \lambda_R) + I(\vec{r}_\perp, z, \lambda_G) + I(\vec{r}_\perp, z, \lambda_B),$$

where the monochromatic images are given by

$$I(\vec{r}_\perp, z, \lambda_j) = |E(\vec{r}_\perp, z, \lambda_j)|^2, \quad j = R, G, B.$$

When verifying the correctness of our model, data measured from a single cuticle cell were used in the diffraction integral, and the color images obtained by numerical reconstruction and optical measurement were compared. The color images optically measured at different distances from the cuticle of *Chrysina gloriosa* are shown in Fig. 5(a). The color of the central disk, which is orange at the shortest distance, changes to yellow and then green at greater distances. This axial coloration agrees well with the results of the proposed model shown in Fig. 5(b). The intensity spots I_{RGB} reconstructed at distances $z = 0.1 \mu\text{m}$, $0.3 \mu\text{m}$,

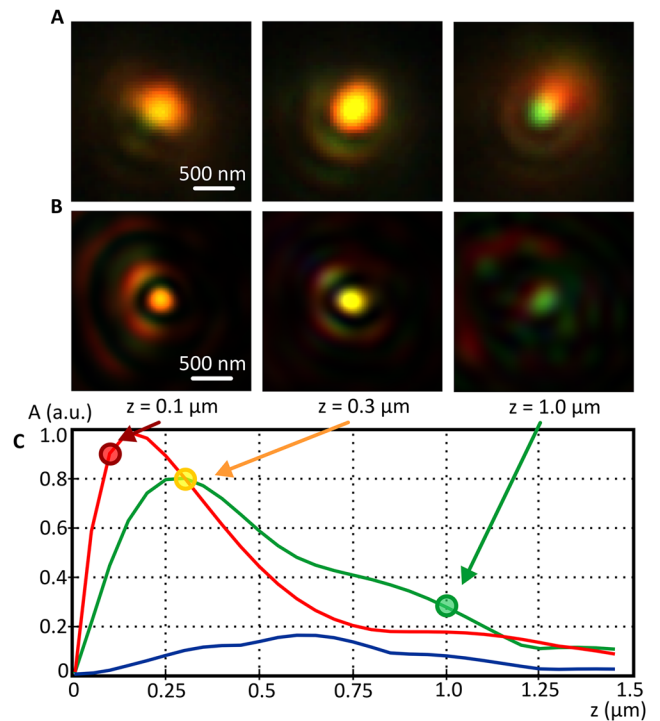


FIG. 5. Colors of the Bessel beam shaped by *Chrysina gloriosa* at different distances from the cuticle. (a) Color image spots obtained by optical measurements. (b) Color image spots numerically reconstructed from the measured amplitude and phase of a single axicon cell. (c) Change in the weighted axial intensity of the R, G, and B colors of the numerically reconstructed Bessel beams as a function of the distance from the cuticle.

and $1\ \mu\text{m}$ from the cuticle represent the incoherent superposition of the images $I(\lambda_j)$ obtained for the wavelengths $\lambda_R = 700\ \text{nm}$, $\lambda_G = 546.1\ \text{nm}$, and $\lambda_B = 435.8\ \text{nm}$. The monochromatic images were calculated numerically from the Kirchhoff diffraction integral using the amplitude A and phase $\Delta\Phi$ measured in a single axicon cell. The weighting coefficients of the monochromatic images used in the superposition were calculated for $M = 3$ and the optical thickness of the layers $\delta_1 = 0$, $\delta_2 = \delta_3 = 1.2\ \lambda_G$, which resulted in the normalized values $|w(\lambda_R)|^2 = 1.00$, $|w(\lambda_G)|^2 = 0.65$, and $|w(\lambda_B)|^2 = 0.15$. The optically measured image spots differ slightly from those that were numerically reconstructed in that they have larger central disks and less distinct surrounding rings. Via numerical reconstruction, the response of the measured axicon cell was obtained for a single plane wave, which was unattainable by optical measurement. Although a pinhole with a diameter of $100\ \mu\text{m}$ was used as an aperture diaphragm for the Köhler illumination, the cell was still illuminated by a set of slightly inclined plane waves. As a result, the inclined plane waves formed laterally shifted Bessel beams which overlapped each other, increasing the diameter of the central disk and blurring the rings (supplementary material, Figs. S3 and S4). The coloring of the rings and the axial color change in the central disk show good agreement between the numerical reconstruction and the optical measurements. According to our model, these effects appear as a result of the different spatial intensity distributions of the Bessel beams created by R , G , and B colors of light. This is well demonstrated by the different changes in the calculated axial intensities with distance z from the cuticle, shown in Fig. 5(c). In a coordinate system whose origin is at the center of the axicon cell, the individual curves represent the weighted axial intensity of each color, determined by $I(|\vec{r}_\perp| = 0, z, \lambda_j)$ with $j = R, G, B$. The color image spot reconstructed at the distance $z = 0.1\ \mu\text{m}$ [position (a)] is composed of monochromatic beams whose weighted axial intensity is dominated by the R channel, with the G and B channels being significantly weaker and completely negligible, respectively; hence, the central disk is orange. At $z = 0.3\ \mu\text{m}$ [position (b)], the weighted axial intensities of the R and G channels are just balanced while the B channel remains weak, making the central disk yellow in color. At $z = 1.0\ \mu\text{m}$, the dominance of the G channel results in the green color of the central disk.

IV. DISCUSSION AND CONCLUSIONS

In conclusion, we have demonstrated high-resolution phase measurement of jewel scarabs, clarifying the light shaping in the cuticle. The spatially structured cells forming the cuticle have been shown to be micrometer-sized reflective axicons that generate nondiffracting Bessel beams. These cuticle biomodulators provide remarkable optical performance, competitive with the high-aperture meta-axicons recently designed for generating subwavelength Bessel beams.²⁹ The comparison of natural and technologically advanced axicons is instructive, both in terms of light control mechanisms and of the limitations in achieving the highest numerical aperture.

The shaping of light by a meta-axicon is implemented through spatial variation of the geometric phase that accompanies transformation of the polarization state. The dielectric meta-axicon is formed by regularly spaced TiO_2 nanofins acting as a half-wave plate reversing the handedness of the circular polarization of the incident

light. The angle of the anisotropy axis of the half-wave plate (the nanofin angular orientation) is a free parameter that changes the geometric phase. By precisely adjusting the nanofin angle at each spatial position, the incident collimated light is deflected by a particular angle relative to the meta-axicon axis to form the Bessel beam. The deflection angle θ defines the numerical aperture of the meta-axicon, $NA_a = \sin \theta$, and determines the full width at half maximum of the Bessel beam, $FWHM = 0.358\lambda/NA_a$.²⁹ The geometric phase of light is sampled by a set of spatially separated nanofins; hence, the conversion efficiency of the meta-axicon decreases with increasing deflection angle, which limits the numerical aperture. A numerical aperture $NA_a = 0.9$ was demonstrated for a meta-axicon designed for $\lambda = 405\ \text{nm}$, generating a zero-order Bessel beam with $FWHM \cong 160\ \text{nm}$.

In the jewel scarab cuticle, the chitin layers create a helicoidal structure responsible for the polarization anomalous (helicity-preserving) reflection. The monochromatic white light components reflected by the individual layers interfere and their optical paths vary spatially, resulting in phase modulation (the phase associated with the optical path length is referred to as dynamic phase). The modulation of the dynamic phase is introduced by wax filled axicon cells forming the outer cuticle whose shape is replicated also in underlying chitin layers. Unlike meta-axicons, where the geometric phase is spatially sampled, the cuticle axicons change the dynamic phase continuously. As a result of this modulation, jewel scarabs can create a regular high-resolution structure of axicons whose diameter of $6\ \mu\text{m}$ is 50 times smaller than that of the meta-axicon. The achievable numerical aperture is limited by the total reflection and is favorably affected by the wax filling of the axicon cells. The measurements show that the axicon parameters are combined to achieve the highest possible numerical aperture ($NA_a = 0.9$), providing the smallest spot size in the generated Bessel beam ($FWHM \cong 200\ \text{nm}$ for $\lambda = 500\ \text{nm}$). Despite the differing physical constraints, the highest numerical aperture is the same for both the cuticle axicons and the meta-axicons and significantly exceeds the numerical aperture achievable with conventional refractive axicons ($NA_a = 0.75$). The high-resolution phase imaging showed that individual axicon cells have a rounded tip. This is disadvantageous because such a tip produces light which interferes with the Bessel beam formed. Undesirable interference causes oscillations in the axial intensity of the Bessel beam and affects the stability of its transverse intensity profile.³³ Phase measurements showed a nearly symmetric axicon shape of the cells, allowing generation of beams that closely approached ideal nondiffracting Bessel beams. The quality of these beams was verified by both direct observation and numerical reconstruction from the measured phase and was even sufficient to demonstrate self-healing from amplitude and phase perturbations. Under Köhler illumination, individual cuticle cells create bright image spots that arise from incoherent superposition of laterally shifted Bessel beams. Compared to a single Bessel beam, this composite spot is larger in size and secondary concentric rings are missing. With dark field illumination using only the inclined waves, on axis Bessel beams are not created and annular image spots with a dark center are observed. The change of the cuticle image with illumination was previously demonstrated,⁸ and we explain this effect in the supplementary material.

The demonstrated abilities of jewel scarabs inspire the development of new polarization-sensitive light-shaping technologies,

combining polarization-selective reflection and multibeam interference with spatial light modulation that is performed without the sampling required by artificially prepared metasurfaces or diffractive elements. This opens pathways for high-quality light shaping and preparation of special states of light at the microscale. Mimicking the subwavelength Bessel beams generated by jewel scarabs, the structural coloration, axial color conversion, or self-imaging of Bessel beams^{34,35} may be used as sensitive indicators that enable phase measurement or colorimetric refractive index sensing.

SUPPLEMENTARY MATERIAL

See the [supplementary material](#) for a quantitative phase imaging by geometric-phase microscopy and comparison of the measurement with scanning electron microscopy. In addition, non-diffracting Bessel beams and self-healing effect are described, and the dependence of microscopic images of cuticle cells on the illumination conditions is explained.

ACKNOWLEDGMENTS

We acknowledge funding from the Grant Agency of the Czech Republic (Grant Nos. GA18-01396S and GA18-05770S), the Ministry of Education, Youth and Sports (MEYS) (No. LM2015062 Czech-BioImaging), the H2020 Twinning project SINNCE (Grant No. 810626), and CEITEC 2020 (Grant No. LQ1601) with financial support from the MEYS CR under the National Sustainability Programme II. P.B. was supported by a scholarship awarded by the Czechoslovak Microscopy Society.

P.B. and Z.B. report a Czech patent, No. 307520, and pending PCT application for the geometric-phase microscope used in the submitted study.

REFERENCES

- ¹M. Srinivasarao, *Chem. Rev.* **99**, 1935 (1999).
- ²P. Vukusic and J. R. Sambles, *Nature* **424**, 852 (2003).
- ³A. A. Michelson, *London, Edinburgh, Dublin Philos. Mag. J. Sci.* **21**, 554 (1911).
- ⁴D. H. Goldstein, *Appl. Opt.* **45**, 7944 (2006).
- ⁵Y. Bouligand, *C. R. Chim.* **11**, 281 (2008).
- ⁶V. Sharma, M. Crne, J. O. Park, and M. Srinivasarao, *Mater. Today: Proc.* **1**, 161 (2014).
- ⁷A. Pace, *Science* **176**, 678 (1972).
- ⁸V. Sharma, M. Crne, J. O. Park, and M. Srinivasarao, *Science* **325**, 449 (2009).
- ⁹H. de Vries, *Acta Crystallogr.* **4**, 219 (1951).
- ¹⁰W. E. Vargas, M. Hernández-Jiménez, E. Libby, D. E. Azofeifa, C. Barboza, and Á. Solís, *Opt. Photonics J.* **06**, 146 (2016).
- ¹¹G. Agez, C. Bayon, and M. Mitov, *Acta Biomater.* **48**, 357 (2017).
- ¹²A. Mendoza-Galván, L. F. del Río, K. Järrendahl, and H. Arwin, *Sci. Rep.* **8**, 6456 (2018).
- ¹³C. Q. Cook and A. Amir, *Optica* **3**, 1436 (2016).
- ¹⁴A. Sweeney, C. Jiggins, and S. Johnsen, *Nature* **423**, 31 (2003).
- ¹⁵N. J. Marshall, S. B. Powell, T. W. Cronin, R. L. Caldwell, S. Johnsen, V. Gruev, T.-H. S. Chiou, N. W. Roberts, and M. J. How, *J. Exp. Biol.* **222**, jeb134213 (2019).
- ¹⁶D. H. Goldstein, *Polarized Light* (CRC Press, 2017).
- ¹⁷S. Tadeipalli, J. M. Slocik, M. K. Gupta, R. R. Naik, and S. Singamaneni, *Chem. Rev.* **117**, 12705 (2017).
- ¹⁸S. Vignolini, P. J. Rudall, A. V. Rowland, A. Reed, E. Moyroud, R. B. Faden, J. J. Baumberg, B. J. Glover, and U. Steiner, *Proc. Natl. Acad. Sci. U. S. A.* **109**, 15712 (2012).
- ¹⁹L. F. del Río, H. Arwin, and K. Järrendahl, *Thin Solid Films* **571**, 410 (2014).
- ²⁰M. Mitov, V. Soldan, and S. Balor, *Arthropod Struct. Dev.* **47**, 622 (2018).
- ²¹Y. Bouligand, *Tissue Cell* **18**, 621 (1986).
- ²²S. Taqi, S. Sami, L. Sami, and S. Zaki, *J. Oral Maxillofac. Pathol.* **22**, 279 (2018).
- ²³S. Valyukh and K. Järrendahl, *Appl. Opt.* **56**, 2510 (2017).
- ²⁴D. McGloin and K. Dholakia, *Contemp. Phys.* **46**, 15 (2005).
- ²⁵P. Bouchal, P. Dvořák, J. Babočky, Z. Bouchal, F. Ligmajer, M. Hrtoň, V. Křápek, A. Faßbender, S. Linden, R. Chmelík, and T. Šikola, *Nano Lett.* **19**, 1242 (2019).
- ²⁶P. Bouchal, L. Štrbková, Z. Dostál, R. Chmelík, and Z. Bouchal, *Sci. Rep.* **9**, 3608 (2019).
- ²⁷S. A. Jewell, P. Vukusic, and N. W. Roberts, *New J. Phys.* **9**, 99 (2007).
- ²⁸D. E. Azofeifa, M. Hernández-Jiménez, E. Libby, A. Solís, C. Barboza-Aguilar, and W. E. Vargas, *J. Quant. Spectrosc. Radiat. Transfer* **160**, 63 (2015).
- ²⁹W. T. Chen, M. Khorasaninejad, A. Y. Zhu, J. Oh, R. C. Devlin, A. Zaidi, and F. Capasso, *Light: Sci. Appl.* **6**, e16259 (2017).
- ³⁰Z. Bouchal, J. Wagner, and M. Chlup, *Opt. Commun.* **151**, 207 (1998).
- ³¹V. Garcés-Chávez, D. McGloin, H. Melville, W. Sibbett, and K. Dholakia, *Nature* **419**, 145 (2002).
- ³²F. O. Fahrbach, P. Simon, and A. Rohrbach, *Nat. Photonics* **4**, 780 (2010).
- ³³O. Brzobohatý, T. Čižmár, and P. Zemánek, *Opt. Express* **16**, 12688 (2008).
- ³⁴S. Chávez-Cerda, M. A. Meneses-Nava, and J. M. Hickmann, *Opt. Lett.* **23**, 1871 (1998).
- ³⁵M. Fortin, M. Piché, and E. F. Borra, *Opt. Express* **12**, 5887 (2004).